Neurobiology of Aging 75 (2019) 1–10

Contents lists available at ScienceDirect

Neurobiology of Aging

journal homepage: www.elsevier.com/locate/neuaging

Loss of PINK1 causes age-dependent decrease of dopamine release and mitochondrial dysfunction

Lianteng Zhi [a], Qi Qin [a], Tanziyah Muqeem [a], Erin L. Seifert [b], Wencheng Liu [c], Sushuang Zheng [d], Chenjian Li [d,*], Hui Zhang [a,**]

[a] Department of Neuroscience, Thomas Jefferson University, Philadelphia, PA, USA
[b] Department of Pathology, Thomas Jefferson University, Philadelphia, PA, USA
[c] Department of Neurology and Neuroscience, Weill Medical College of Cornell University, New York, NY, USA
[d] School of Life Sciences, Peking University, Beijing, China

ARTICLE INFO

Article history:
Received 17 September 2017
Received in revised form 30 September 2018
Accepted 26 October 2018
Available online 2 November 2018

Keywords:
PINK1
Dopamine release
Parkinson's disease
Mitochondria dysfunction
Mitochondria respiration
Fast-scan cyclic voltammetry

ABSTRACT

Mutations and deletions in PTEN-induced kinase 1 (PINK1) cause autosomal recessive Parkinson's disease (PD), the second most common neurodegenerative disorder. PINK1 is a nuclear-genome encoded Ser/Thr kinase in mitochondria. PINK1 deletion was reported to affect dopamine (DA) levels in the striatum and mitochondrial functions but with conflicting results. The role of PINK1 in mitochondrial function and in PD pathogenesis remains to be elucidated thoroughly. In this study, we measured DA release using fast-scan cyclic voltammetry in acute striatal slices from both PINK1 knockout (KO) and wild-type (WT) mice at different ages. We found that single pulse-evoked DA release in the dorsal striatum of PINK1 KO mice was decreased in an age-dependent manner. Furthermore, the decrease was because of less DA release instead of an alteration of DA transporter function or DA terminal degeneration. We also found that PINK1 KO striatal slices had significantly lower basal mitochondria respiration compared with that of WT controls, and this impairment was also age-dependent. These results suggest that the impaired DA release is most likely because of mitochondrial dysfunction and lower ATP production.

1. Introduction

Parkinson's disease (PD) is the most common neurodegenerative disease, caused by in part a progressive loss of dopamine (DA) neurons within the substantia nigra pars compacta and a subsequent deficiency of the neurotransmitter DA in the striatum (STR) (Dauer and Przedborski, 2003). The occurrence is mostly sporadic, although mutations in twenty genes have been linked to genetic forms of PD (Hewitt and Whitworth, 2017). Homozygous and compound heterozygous mutations in the PINK1 gene are the second most frequent cause of autosomal recessive early-onset Parkinsonism (Valente et al., 2004a,b). PINK1 is a ubiquitously expressed serine/threonine kinase with high levels in the heart, skeletal muscle, and the brain. It also contains a mitochondrial targeting sequence in the N-terminus that directs import of PINK1 into mitochondria, suggesting a role in mitochondrial function. Previous studies have shown that early-onset Parkinsonism–associated mutations have reduced PINK1 kinase activity. Hence, several PINK1 knockout (KO) mouse models were generated to study the pathogenic mechanisms of PD (Akundi et al., 2011; Gispert et al., 2009; Heeman et al., 2011; Kitada et al., 2007).

Although all the PINK1 KO mouse models so far lack overt neurodegeneration, previous studies have shown that PINK1 deletion can alter DA levels in the STR, supporting the notion that synaptic dysfunction occurs before neurodegeneration or behavior deficits. Nevertheless, it is controversial whether DA release is decreased or not. Most of the studies measured DA levels using HPLC which provides little information of phasic DA release and kinetics. Kitada et al. revealed that single pulse (1p)–evoked DA overflow was significantly decreased in PINK1 KO mice at 2–3 months old and attributed this alteration to decreased DA transporter (DAT) function using amperometric recordings (Kitada et al., 2007). On the contrary, a recent finding reported unaltered striatal DA release in 2-month-old PINK1 KO mice using fast-scan cyclic voltammetry (FSCV) recording, and no alteration of DAT functions (Sanchez et al., 2014). The PINK1 KO rats, the only rodent

* Corresponding author at: School of Life Sciences, Peking University, Beijing 100871, China. Tel.: +86-10-6275-6459.
** Corresponding author at: Department of Neuroscience, Thomas Jefferson University, Philadelphia, PA 19107, USA. Tel.: +215-503-7213; Fax: +215-955-4949.
E-mail addresses: li_chenjian@pku.edu.cn (C. Li), hui.x.zhang@jefferson.edu (H. Zhang).

0197-4580/$ – see front matter © 2018 Elsevier Inc. All rights reserved.
https://doi.org/10.1016/j.neurobiolaging.2018.10.025

model which exhibited significant motor deficits and substantia nigra pars compacta DA neuron degeneration at 8 months of age paradoxically showed a 2 to 3-fold increase in striatal DA content measured by HPLC (Dave et al., 2014). Because the previous results were not consistent with one another, it is important to know how DA release is altered in PINK1 KO mice, whether the alteration is age-dependent, and whether and how mitochondria are involved in DA release.

Aberrant mitochondrial function has long been implicated in the pathogenesis of PD (Hauser and Hastings, 2013; Moon and Paek, 2015; Perier and Vila, 2012; Van Laar and Berman, 2013) and PINK1 is believed to exert neuroprotection by maintaining mitochondrial integrity (Clark et al., 2006; Narendra and Youle, 2011; Steer et al., 2015). PINK1 KO/KD fibroblasts and neurons display reduced mitochondrial membrane potential (MMP), impairment in respiration, ATP reduction, calcium overload, and heightened reactive oxygen species production (Gandhi et al., 2009, 2012; Gautier et al., 2008, 2012; Heeman et al., 2011; Kostic et al., 2015; Liu et al., 2011; van der Merwe et al., 2017; Wang et al., 2011). Mitochondria isolated from STR or whole brain of aged PINK1 KO mouse show defects in complex I (Gautier et al., 2008; Liu et al., 2011; Morais et al., 2009, 2014). Directly measuring the oxygen consumption rate (OCR) is one of the most popular methods to evaluate mitochondrial function. Previous studies demonstrated an altered mitochondrial respiration rate in isolated mitochondria or primary cultures from PINK1 KO mice, but the results are controversial. One report described that respiratory activity was reduced for both complex I and complex II in isolated mitochondria from STR of PINK1 KO mice at the age of 3–4 months, and increased sensitivity to oxidative stress, but no change for the basal OCR (Gautier et al., 2008). In another study, Gispert found a reduction of respiratory activities for complexes I+III+IV and IV in purified mitochondria from 18-month-old brain tissue of mice (Gispert et al., 2009). Some studies reported increased basal OCR (Akundi et al., 2011; Cooper et al., 2012; Villeneuve et al., 2016), whereas others showed decreased OCR (Liu et al., 2011; Morais et al., 2014). The discrepancy could be either due to different tissues and cells preparation, different measuring methods, or due to loss of physiological condition in isolated mitochondria. The Seahorse Extracellular Flux (XF24) analyzer is a commonly used tool for measuring oxygen consumption in cell cultures or purified mitochondria which offers improved throughput compared with traditional O_2 electrode–based methods (Gerencser et al., 2009). It can also be adapted to study acute brain slices (Fried et al., 2014). In the present study, we have developed a method to measure mitochondrial respiration using XF24 analyzer in acute striatal slices. We found that the basal OCR and ATP production are decreased in the aged PINK1 KO mice. The decrease of mitochondrial respiration is age-dependent, correlated with the age-dependent decreased evoked DA release in the STR. The mitochondrial coupling efficiency was impaired in the PINK1 KO mice from a young age, which might accumulate with age leading to the observed reduced ATP production and reduced DA release later on.

2. Methods

2.1. Animals

All animal work has been conducted according to national and international guidelines and has been approved by the Animal Care and Use Committee of the Cornell Medical School and Thomas Jefferson University.

2.2. Materials

Bovine serum albumin (BSA) (A6003), glucose (G8270), sodium pyruvate (P2256), L-glutamine (C3126), oligomycin from streptomyces diastatochromogenes (O4876), carbonyl cyanide 4-(trifluoromethoxy) phenylhydrazone (FCCP) (C2920), and antimycin A from streptomyces sp. (A8674) were purchased from Sigma Aldrich (St. Louis, MO); rotenone (3616) was from Tocris; stainless steel biopsy punches were from Miltex (York, PA); and XF24 Islet FluxPaks were purchased from Seahorse Bioscience (Billerica, MA).

2.3. Generation of PINK1 KO mice

The genomic murine PINK1 gene was used to generate a targeting construct in which PINK1 gene from exon 2 to exon 5 were replaced with a LacZ/Neo cassette (Fig. S1). Targeting constructs were transfected into embryonic stem cells of C57BL/6 ×129/SvEv background. After selected with neomycin, G418-resistant ES colonies were screened by PCR to confirmed the correct genetic manipulation. PCR-positive colonies were also confirmed by Southern blotting of BgII- or AvrII-digested genomic DNA by using PINK1 5′ internal probe and 3′ external probe. Successful homologous recombinants were injected into day 3.5 C57BL/6 blastocytes to generate chimeric mice. Three chimeric founders 1A2, 1B3, and 1D6 were confirmed by PCR with primers (Primer 26: 5′-ATGA GATGGAGGGGAGTCCT-3′; Primer Neo3A: 5′GCAGCG CAT CGC CTT CTA TC-3′). Sequencing of the specific PCR products confirmed the correct targeting event. Founders were bred to test the germ-line transmission and confirmed by Southern blotting of tail genomic DNA digested by SacI and probed with IRES8/9 which is internal to LacZ-Neo cassette. F1 offspring were used to breed to homozygosity and backcrossed for eight generations to FVB/NTac mice. Genotypes of animals were verified by using PCR (Primer-26: 5′-ATGA GATGGAGGGGAGTCCT-3'; primer-27: 5′-GGAAGG AGG CCA TGG AAA TTG T-3′; Primer-Neo3A: 5′GCAGCG CAT CGC CTT CTA TC-3′), for the presence of KO alleles and absence of the wild-type allele. PCR conditions were 95 °C for 2 minutes, 95 °C for 20 seconds, 51 °C for 20 seconds, 72 °C for 20 seconds (35 cycles), and 72 °C for 5 minutes. Brain extracts from homozygous PINK1 KO mice was tested by RT-PCR and western blot with anti-PINK1 antibody (a gift from Eli Lilly Inc), and confirmed that PINK1 mRNA and protein were absent in the PINK1 KO mice (Fig. S1D and E).

2.4. RNA extraction, cDNA synthesis, and RT-PCR

For the analysis of PINK1 knockdown efficiencies, quantitative RT-PCR was performed to detect mRNA level in PINK1 KO mice. Total RNA from PINK1 KO and WT control mice was isolated using TRIzol reagent (Sigma-Aldrich) and treated with DNase I (Qiagen). cDNA was synthesized using random primers according to manufacturer's instructions (Thermo Scientific). cDNA was diluted 1:5 in water before PCR and was measured by quantitative PCR with SYBR Green I kit according to manufacturer's instruction (Bio-Rad). For quantitative PCR, the following primers were used: mouse PINK1 primers 5′-TTGCAATGCCGCTGTGTATG-3′ (forward) and 5′-TGGAG GAACCTGCCGAGATA-3′ (reverse); internal control mouse β-actin primers 5′-CTGTCCCTGTATGCCTCTG-3′ (forward) and 5′-ATGT CACGCACGATTTCC-3′ (reverse). PCR was performed by using Bio-Rad CFX96 qPCR system.

2.5. Acute striatal slice preparation

Animals were decapitated after cervical dislocation and brains were immediately dissected out in cold preoxygenated cutting solution (in mM: 125 NaCl, 2.5 KCl, 26 $NaHCO_3$, 3.7 $MgSO_4$, 0.3

KH_2PO_4, 10 glucose, pH 7.4). Coronal striatal slices were sectioned with a vibrating microtome (VT1200; Leica, Solms, Germany) at a thickness of 300 μm and recovered in oxygenated artificial cerebrospinal fluid (ACSF, in mM, 125 NaCl, 2.5 KCl, 26 $NaHCO_3$, 2.4 $CaCl_2$, 1.3 $MgSO_4$, 0.3 KH_2PO_4, 10 glucose, 2 HEPES, pH 7.4) at room temperature for 1.5 hours.

For mitochondria respiration experiments, 150-μm slices were prepared, then transferred to respiration buffer (preoxygenated ACSF with 25 mM glucose, 2 mM L-glutamine, and 4 mg/mL BSA, added freshly before use, pH 7.4 at 37 °C), and punched immediately for slice respiration study or incubated for 2 hours for later slice evaluation analysis, such as propidium iodide (PI) staining, FSCV recording, or patch clamp recording (ACSF/BSA group), with the continuously oxygenated slices as control (control group).

2.6. Fast-scan cyclic voltammetry recording

FSCV and amperometry were used to measure evoked DA release in dorsal STR. Slices were placed in a recording chamber, and superfused (1 mL/min) with ACSF at 36 °C. Electrochemical recordings and electrical stimulation were performed as previously described (Zhang and Sulzer, 2003). In brief, freshly cut carbon fiber electrodes ~5 μm in diameter were inserted into the dorsal STR ~50 μm into the slice. For FSCV, a triangular voltage wave (−400 to +900 mV at 280 V/s vs. Ag/AgCl) was applied to the electrode every 100 ms, and current recorded using an Axopatch 200B amplifier (Axon Instrument, Foster City, CA), with a low-pass Bessel Filter set at 10 kHz, digitized at 25 kHz (ITC-18 board, Instrutech Corporation, Great Neck, New York). Slices were electrically stimulated every 2 minutes with different stimulation paradigm using a bipolar stimulating electrode ~100 μm from the recording electrode. For KCl-evoked DA release, ACSF containing 70 mM KCl was applied. Background-subtracted cyclic voltammograms identified the released substance as DA. The DA oxidation current was converted to concentration based on a calibration of 5 μM DA in ACSF after the experiment.

2.7. Propidium iodide staining and fluorescence imaging

Slices from both ACSF/BSA and control group were incubated in preoxygenated ACSF with 10 μM PI and 10 μM Hoechst 33258 for 15 minutes at room temperature, followed by two times of wash with ACSF, and then 4% PF fixation for 20 minutes. PI and Hoechst 33258 fluorescence was imaged using an Olympus confocal imaging microscope (FV10-ASW, Olympus, Tokyo, Japan) at 60 μm beneath the surface for the ACSF/BSA and control group. The number of dead (PI labeled) and total cells (Hoechst 33258 labeled) was counted, and live cell percentage was calculated.

2.8. Patch clamp recording

Whole-cell patch clamp recordings were performed on layers V mPFC pyramidal neurons and medium spiny neurons (MSNs) in the dorsal STR through an upright Olympus BX50WI (Olympus, Tokyo, Japan) differential interference contrast microscope with a 40× water immersion objective and an IR-sensitive video camera. All experiments were conducted at 36 °C. For the recording, slices were submerged in a perfusion of ACSF (2 mL/min). Pipettes (3–5 MΩ) were filled with (in mM): 115 K-gluconate, 10 HEPES, 2 $MgCl_2$, 20 KCl, 2 MgATP, 1 Na_2-ATP, 0.3 GTP, pH 7.3; 280 ± 5 mOsm.

Whole-cell patch clamp recording were performed with a multiclamp 700B amplifier (Molecular Devices, Forster City, CA) and digitized at 10 kHz with a Digidata 1440A (Molecular Devices). Data were acquired using the Clampex 10.2 software (Molecular Devices) for subsequent analysis. In each cell, input resistance (measured by 100 pA, 100 ms duration hyperpolarizing pulses), membrane potential, the number of evoked spikes, and the latency to the first spike evoked by a 500-ms duration depolarizing current pulse (150–450 pA) were injected at 1-minute interval and analyzed.

2.9. Mitochondrial respiration study

Different combination of slice thickness (150 μm or 200 μm) and punch size (1.0 mm, 1.5 mm, and 2.0 mm) were chosen to optimize the slice condition for the measurement of OCR. Slices were attached to the center of mesh in the islet capture plate, similar to the previously mentioned (Fried et al., 2014). The microplate was then incubated at 37 °C for 1 hour to allow for temperature and pH equilibration.

The drugs/inhibitors were diluted in 37 °C respiration buffer to the stock concentration (10 X, 11 X, 12 X, and 13 X of working concentration, respectively, from port A to D) and then preloaded into the reagent ports A, B, C, and D of the sensor cartridge that had been hydrating in Seahorse calibration solution overnight at 37 °C (without CO_2). The injection volume was 75 μL. After 30-minute calibration and the following equilibration, the oxygen consumption in each well of the plate was measured with the program 3-min mix, 3-min wait, and 2-min measure sequences, and the OCR was calculated. Our experiments included 4 OCR measurements to create a baseline, followed by the injection of port A (10 mM pyruvate, 3 X measurements), port B (20 μM Oligomycin, 8 X measurements), port C (10 μM or other concentrations of FCCP, 5X measurements), and port D (20 μM antimycin A, 6 X measurements). The parameters for load, measure, and calibration distance of probe head were 27,800.

2.10. ATP measurement

Acute striatal slices from both PINK1 KO and WT groups were punched and frozen in liquid nitrogen immediately after slicing, then kept in −80 °C freezer for later analysis. The ATP levels in the STR were determined using commercial kit (ATP determination kit, A22066, Thermo-Fisher Scientific, MA, USA). In brief, 100 μL of ice-cold lysis buffer (in mM: 10 Tris-HCl pH 7.5, 100 NaCl, 1 EDTA, and 0.01% Triton X-100) was added per 10 mg STR sample, and homogenized for 30 seconds using motorized pellet pestle. Ninety μL of homogenate was transferred to new tube and extracted with phenol-chloroform. The water phase was diluted 1:20 for ATP measurement, following the manual of the kit. The ATP levels were compared after normalized with total protein level, measured by the BCA method (Pierce BCA Protein Assay Kit, Thermo Fisher Scientific).

2.11. Immunofluorescence staining and quantification of dopamine axon terminals in the striatum

Mice were sacrificed and then fixed with 4% paraformaldehyde in cold phosphate-buffered saline for 48h; then coronal brain sections at 40-μm thickness were obtained with a vibratome. Serial sections were collected into 10 wells so that each well contained every 10th section. Floating sections were stored in freezing buffer (30% glycerol and 30% ethylene glycol in phosphate-buffered saline) at −20 °C. Floating sections were stained with the monoclonal antityrosine hydroxylase (TH) antibody (Sigma) at a 1:8000 dilution for 36h at 4 °C, then subsequent incubations in Alexa Fluor 488-conjugated secondary antibody (1:500, Life Technologies). Fluorescence images were captured using a laser scanning confocal microscope (63× ZEISS LSM 710 NLO). The paired images in all the figures were collected at the same gain and offset settings. For the

quantitative assessment of TH+ DA axon terminals in the STR sections, images were analyzed by Image-Pro Premier 3D (Media Cybernetics).

2.12. Data analysis and statistics

Values given in the text and in the figures are mean ± SEM. The Student's *t*-test was used for paired data and ANOVA was used for group data (SYSTAT, Systat Software, Inc, San Jose, CA 95131 USA). The difference was considered significant at levels of $p < 0.05$ (*) and $p < 0.01$ (**), $p < 0.001$ (***), and $p < 0.0001$ (****). N stands for the nubmer of mice and n stands for the number of experiments.

3. Results

3.1. Generation and molecular characterization of PINK1 KO mice

To generate PINK1 KO mice, we deleted exons 2-5 in PINK1 gene, so that most of the kinase domain was removed (Fig. S1A). Tail DNA was analyzed by PCR with Neo-vector specific primer and wild-type sequence primer, and the results showed desired gene targeting. Furthermore, DNA sequencing confirmed that the base pair changes were exactly as we designed (Fig. S1B). By genomic Southern blot, we confirmed that only the PINK1 gene was targeted and there was no random insertion of the targeting vector into the genome (Fig. S1C). Finally, RT-PCR analysis of PINK1 mRNA level and western blot of brain extracts from homozygous PINK1 KO mice confirmed that PINK1 mRNA (Fig. S1D) and protein (Fig. S1E) was absent in the PINK1 KO mice.

3.2. Age-dependent decrease of evoked DA release in PINK1 KO striatal slice

To assess directly the vesicular release of DA, we used FSCV (Wightman and Zimmerman, 1990) to measure the kinetics and amount of DA release evoked by a single stimulation (1p) in dorsal STR slices. Owing to the heterogeneity of dopaminergic innervation, the results from three sites in the dorsal STR of each slice were measured and averaged. Compared with control WT littermates, PINK1 KO mice did not show significant alteration in the DA overflow evoked by 1p stimulation in the young group (3–4 month old) (2.6 μM vs. 2.4 μM, Fig. 1A and B, N = 6, n = 15 for WT and KO). By contrast, there was a significant 30% reduction in the DA overflow in the old group (10–14 month old) (2.7 μM vs. 1.9 μM, Fig. 1C and, N = 7, n = 22, for WT and KO, $p < 0.05$). To evaluate whether the decrease was because of less DA synaptic vesicles because of terminal degeneration or less DA packing capacity, we performed KCl-evoked DA overflow experiment which would release all DA (Divito et al., 2015). We did not find any obvious differences in DA overflow in either the young or the old group (Fig. 1E–G). These data indicate that the vesicle pools are not altered and there is no terminal degeneration, consistent with previous studies (Akundi et al., 2011; Gispert et al., 2009; Kitada et al., 2007). There was no difference for the DA terminal density in the STR from WT and KO mice in the old group confirming no degeneration of DA axon terminals in PINK1 KO mice (Fig. 1H).

3.3. The decrease of DA overflow is not because of alteration of DAT function

Because the DA overflow peak obtained reflects the balance of electrically stimulated DA release and reuptake by DAT, we further examined whether the decrease in the old KO group is because of alterations of DA uptake. In the presence of 5 μM cocaine, DAT blocker, the DA release was 25% less in the old PINK1 KO compared with WT controls (4.6 μM vs. 3.3 μM, Fig. 2D and E, N = 4, n = 10 for KO and WT), with a similar pattern of DA decrease as without blockade of DAT. This suggested that the decrease of DA overflow was because of less presynaptic release and not because of alterations of DAT reuptake function. As expected, there was no significant difference for evoked DA release in the presence of cocaine in the young group (3.9 μM vs. 3.7 μM, Fig. 2A and B, N = 6, n = 13). Consistently, the cocaine effect, which was obtained from the ratio of DA overflow at the same site before and after drug treatment, did not show significant difference between PINK1 KO and WT controls in either the young (1.6 vs. 1.7, Fig. 2C, N = 6, n = 13) or the old group (1.8 vs. 1.6, Fig. 2F, N = 4, n = 10). The half-life of the decay phase of the overflow responses evoked by 1p, an indicator of the DAT reuptake, was not different between genotypes of the old group (0.20 ± 0.04 seconds and 0.21 ± 0.05 seconds, WT and KO, respectively; N = 4, n = 10; $p > 0.05$) either.

3.4. DA release from PINK1 KO striatal slices is more vulnerable to FCCP treatment

To evaluate whether the mitochondrial impairment plays a role in the decreased DA release, we treated the slices with 3 μM FCCP, a mitochondrial uncoupler, and measured DA release. FCCP depletes the proton gradient of the mitochondrial membrane and uncouples respiration from ATP synthesis (Brand and Nicholls, 2011). FCCP decreased evoked DA release gradually and induced massive DA release (Fig. 3A and B), and the starting point of massive release could be taken as an index for the vulnerability (Fig. 3A and B). We found that there was no significant difference in the young group (Fig. 3C, N = 6, n = 6), but the starting point was significantly earlier in the PINK1 KO than that of WT control in the old group (Fig. 3D, N = 4, n = 6). No statistical difference was found for the FCCP-induced massive release amplitude in either the young or the old group (Fig. 3E and F). These results are compatible with an age-dependent mitochondrial dysfunction in the PINK1 KO STR, which may be related to the alteration in presynaptic DA release.

3.5. PINK1 KO striatal slices show lower basal respiration levels in age-dependent manner

To directly examine whether there is an alteration of mitochondrial function in KO mice, we used the Seahorse extracellular flux (XF24) analyzer to measure the OCR in acute striatal slices. Because the slices would be incubated in the respiration buffer without oxygenation during the entire duration of measuring (about 4 hours), we sectioned the slice at 150 μm thickness so that O_2 in the ambient air can penetrate the middle of the brain slices with the required oxygen tensions (Humpel, 2015; Jiang et al., 1991). We added 4 mg/mL BSA to the preoxygenated ACSF buffer to facilitate the determination of maximal OCR, as the literature suggests (Schuh et al., 2011). Before the respiration analysis, we first checked whether the slice was healthy under these conditions. The percentage of live cells in both the prefrontal cortex (PFC) and STR were analyzed by PI (10 μM) and Hoechst 33258 (10 μM) double labeling, followed by confocal imaging and cell counting (Fig. S2, N = 3, n = 8). No significant difference was observed between ACSF/BSA group and control group for both the PFC and STR area. We further evaluated whether DA terminals in the striatal slices were functionally healthy by measuring DA release using a battery of tests. We did not find any difference for 1p-evoked release, train pulse stimuli–evoked release, or FCCP-induced massive release vulnerability (Fig. S3). In addition, we assessed whether the neurons under the respiration condition were healthy by patch clamp recording of the pyramidal neurons in the PFC and MSNs in STR (Fig. S4). Neurons were healthy in terms of resting membrane

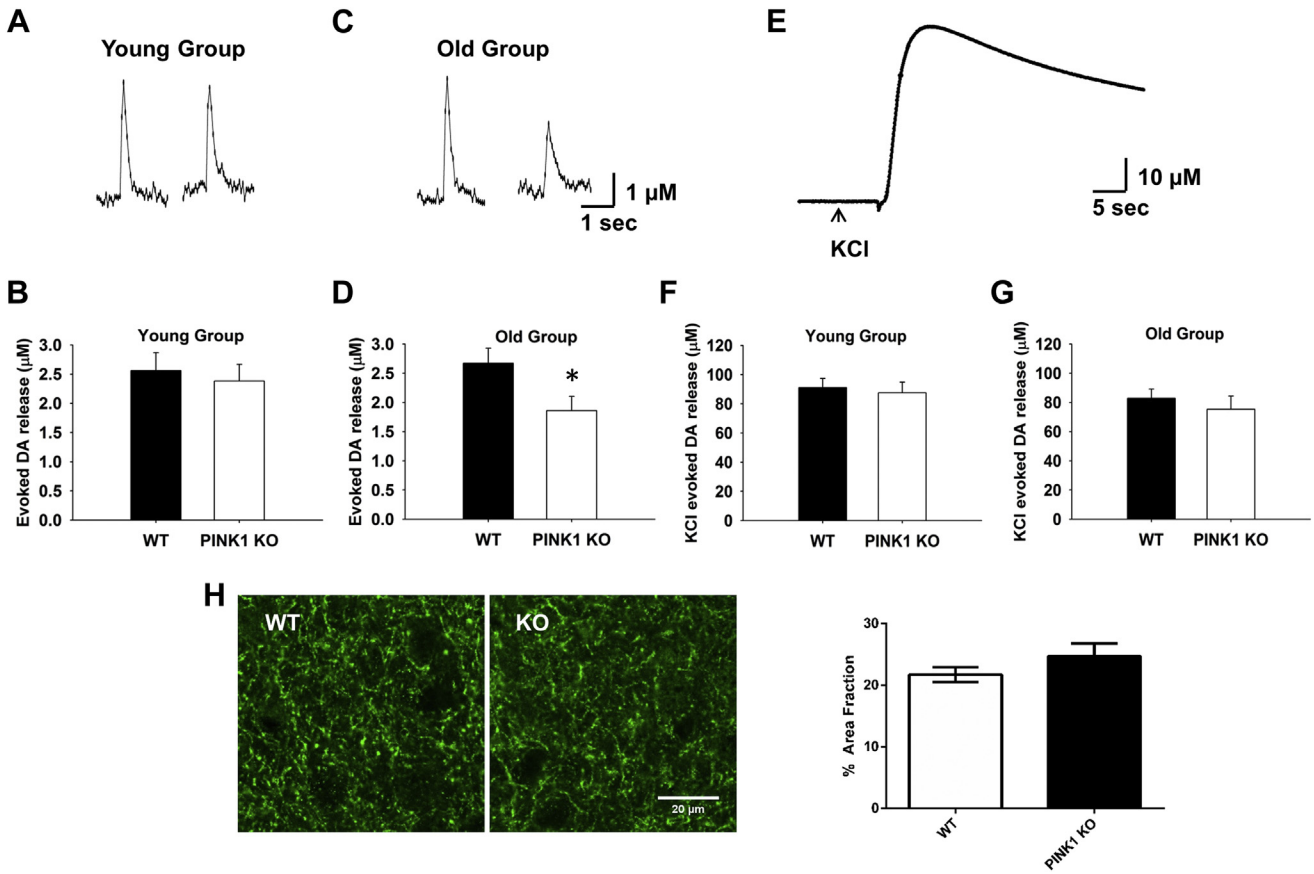

Fig. 1. Age-dependent decrease of evoked DA release in PINK1 KO dSTR slices. Representative traces for 1p-evoked DA release in dSTR slices from both WT and PINK1 KO mice using FSCV were showed for young group (A) and old group (C), respectively. No significant difference of 1p-evoked DA release was found between PINK1 KO and WT in the young group (B, N = 6, n = 15), whereas it was significantly decreased (~30 %) in PINK1 KO in the old group (D, N = 7, n = 22). (E) Representative trace for KCl-evoked total DA release, no significant KCl-evoked DA overflow was found in either young (F, N = 5, n = 19) or old group (G, N = 4, n = 19). (H) No degeneration of DA axon terminals in PINK1 KO mice in the old group. Left panel, representative images of DA axon terminals in the striatum from WT and KO mice labeled by TH; right panel, quantification of TH-labeled DA terminals as fraction of the striatum area (N = 3 for each genotype). * $p < 0.05$. Abbreviations: DA, dopamine; PINK1, PTEN-induced kinase 1; KO, knockout; dSTR, dorsal striatum; WT, wild-type; FSCV, fast-scan cyclic voltammetry; TH, tyrosine hydroxylase.

potential and firing pattern. In summary, the results showed that the health of slice under respiration condition was comparable with the oxygenated control group.

In respiration studies, we first optimized the slice thickness, puncher size, and FCCP concentration for respiration conditions and found that 150-μm thicknesses, 1.5 mm punch size, and 10 μM FCCP condition could give the best read out (Fig. S5). We used this condition to measure the basal OCR for the PINK1 KO mice and WT controls and found age-dependent alteration. The basal OCR was quite similar between different genotypes in the young group (Fig. 4A and B), whereas in the old group, it was significantly decreased in the PINK1 KO slices (Fig. 4D and E). Interestingly, the coupling efficiency was significantly lower in PINK1 KO than that of WT control starting from the young group and remaining significantly lower in the old group (Fig. 4C and F). These results confirmed that PINK1 KO striatal slices had mitochondrial dysfunction, and this dysfunction started from a young age, before the impairment of DA release. We speculate after accumulating defects, the aged PINK1 KO mouse showed decreased basal OCR, which may result in decreased ATP levels in the STR (Amo et al., 2011; Heeman et al., 2011; Liu et al., 2011; Morais et al., 2009). Direct measurement of ATP level in the striatal slices from the old group showed that ATP level was 25% lower in KO compared with WT (2.5 pmol/mg protein vs. 2.0, Fig. 5, N = 7, $p < 0.05$) but not altered in the young group (2.2 pmol/mg protein vs. 2.4, Fig. 5, N = 4, $p > 0.05$).

3.6. Inhibition of ATP generation significantly impairs DA release

Neurotransmission depends on ATP (Billups and Forsythe, 2002; Pathak et al., 2015). Lower basal OCR in aged PINK1 KO mice may cause less ATP production in the STR, which leads to the decreased DA release. Therefore, we tested whether the decrease of DA release is related to ATP levels. We perfused WT striatal slices with 10 μM oligomycin for 20 minutes and measured the DA release every 2 minutes. Inhibition of ATP production by oligomycin resulted in a progressive decrease of DA release (~40 % in the end, Fig. 6A). Similar results were found in 10 μM rotenone (ROT, mitochondria complex I inhibitor) treated slices (Fig. 6B). Treatment of slices with 10 μM oligomycin (Oligo) for 40 minutes resulted in 62.7 ± 4.5% inhibition of evoked DA release (N = 3, n = 6). These results indicate that the decrease of DA release could be attributed to less ATP production because of mitochondria dysfunction in the PINK1 KO mice. Consistently, the inhibition of evoked DA release by oligomycin or rotenone was blunted in the KO mice (N = 3, n = 6, KO vs. KO_ROT vs. KO_Oligo, $p > 0.5$, two-way ANOVA).

4. Discussion

In the present study, we measured extracellular DA overflow using FSCV in acute striatal slices from PINK1 KO and WT mice. We found that 1p-evoked DA release in the dorsal STR of PINK1 KO was

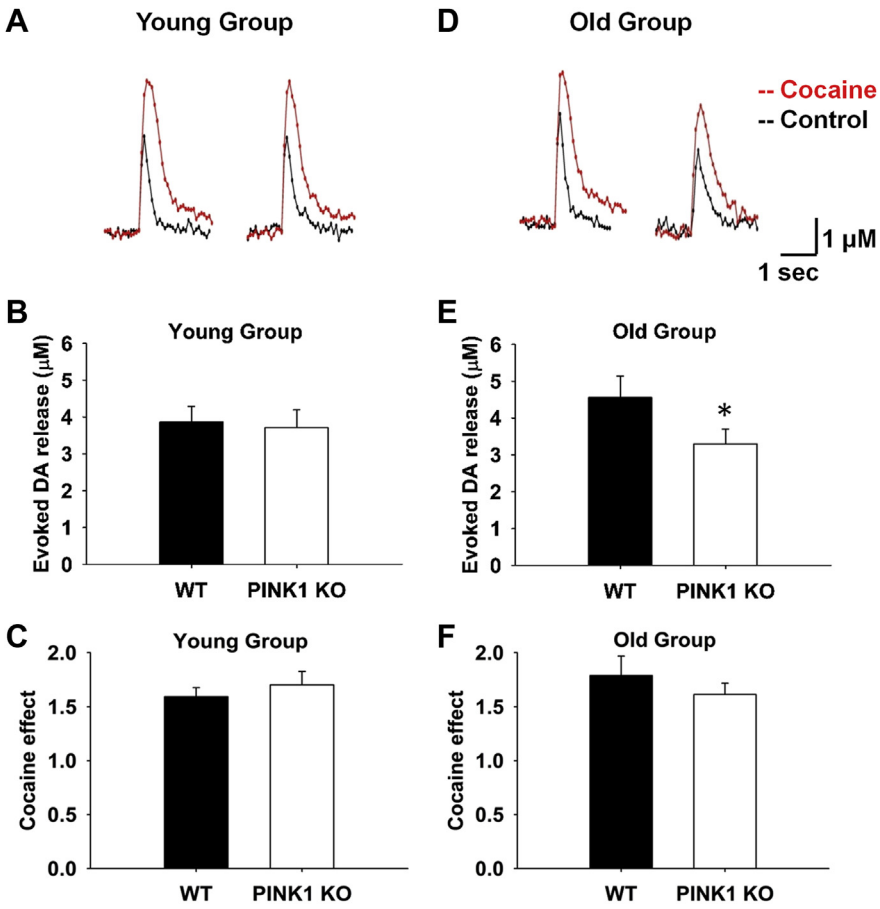

Fig. 2. The decrease of DA overflow is not because of alteration of DAT reuptake function. Representative traces of 1p-evoked DA release were showed in WT and PINK1 KO mice in both young (A) and old group (D), before (black) and after cocaine treatment (red). The young group of PINK1 KO mice did not show obvious decrease of DA release compared with WT controls in the presence of 5 μM cocaine (N = 6, n = 13) (B), whereas in the old group, the PINK1 KO mice showed 25 % less DA release compared with WT controls (E), at a similar decreased level as without DAT blockade (N = 4, n = 10). No significant difference in fold change of DA release were observed after cocaine treatment for PINK1 KO and WT slice in both young (C, N = 6, n = 13) and old group (F, N = 4, n = 10). *$p < 0.05$. Abbreviations: DAT, DA transporter; DA, dopamine; KO, knockout; PINK1, PTEN-induced kinase 1; WT, wild-type.

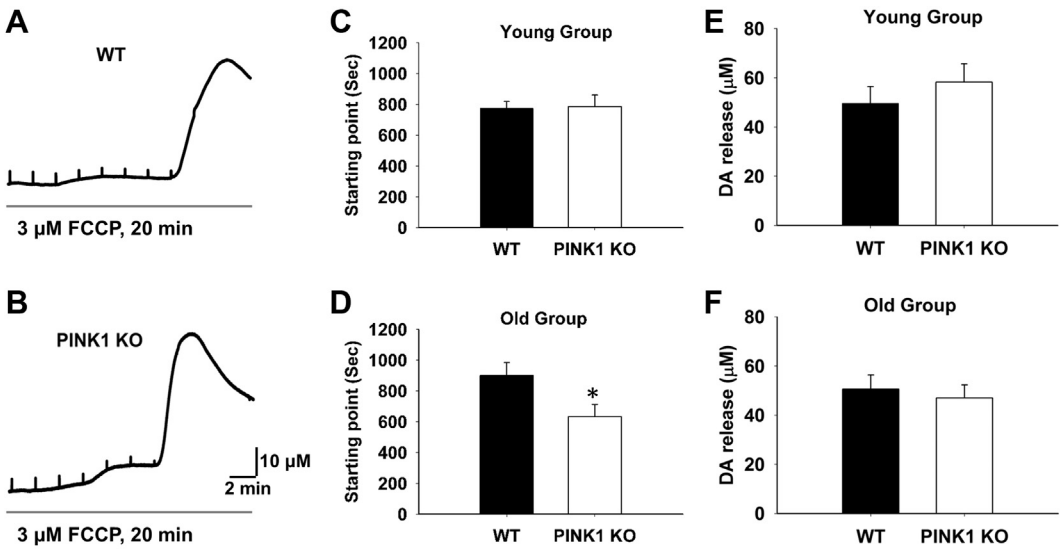

Fig. 3. PINK1 KO slices are more vulnerable to FCCP treatment in the old group. Representative traces of FCCP-induced DA massive release in dSTR slices from WT (A) and PINK1 KO (B) mice. The starting point of mass release did not show significant difference in the young group (C, N = 4, n = 8), whereas was significant earlier for the PINK1 KO slices in the old group (D, N = 4, n = 8). There was no significant alteration of FCCP-induced mass DA release in either young (E) or old group (F). * $p < 0.05$. Abbreviations: FCCP, carbonyl cyanide 4-(trifluoromethoxy) phenylhydrazone; DA, dopamine; KO, knockout; dSTR, dorsal striatum; PINK1, PTEN-induced kinase 1; WT, wild-type.

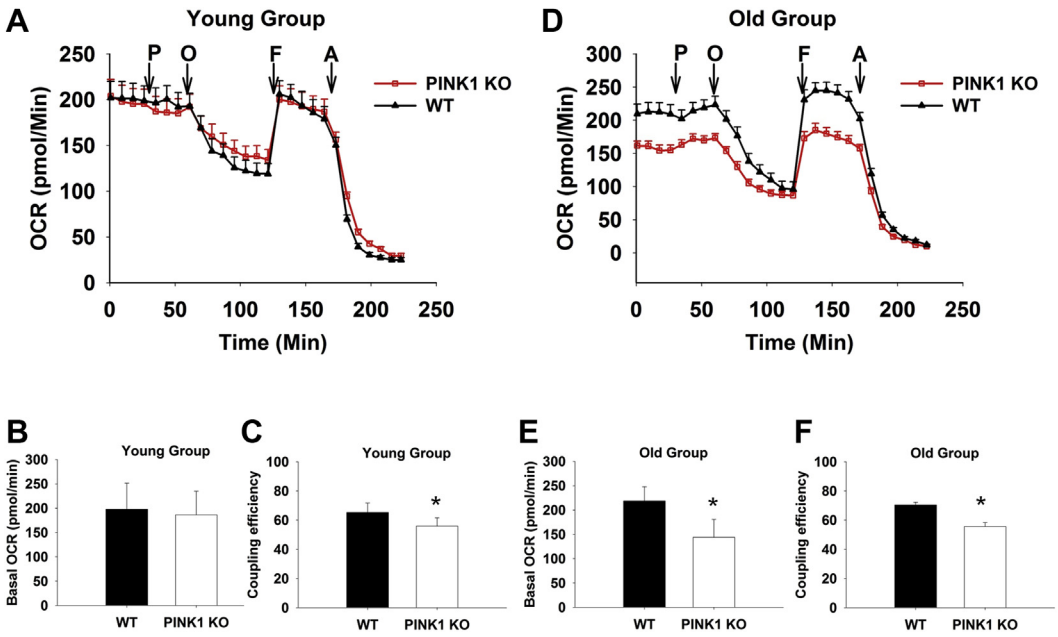

Fig. 4. PINK1 KO slices from old group show significantly lower basal respiration rate. OCRs of acute STR slices (150 μm × 1.5 mm) from both the young (A, B, and C) and the old group (D, E, and F) mice, exposed to successive additions of respiratory modulators (showed in arrows). OCR of the young group was not significantly different between different genotype (B), while the coupling efficiency was decreased in PINK1 KO slices (C). In the old group, the PINK1 KO slices showed a significant decrease of basal respiration level (E) and the coupling efficiency (F). With 10 mM pyruvate (P), 20 μM Oligomycin (O), 10 μM FCCP (F), and 20 μM Antimycin A (A) injected sequentially. N = 4 for each genotype and age. $^{*}p < 0.05$. Abbreviations: PINK1, PTEN-induced kinase 1; KO, knockout; STR, striatum; FCCP, carbonyl cyanide 4-(trifluoromethoxy) phenylhydrazone; OCR, oxygen consumption rate; WT, wild-type.

significantly decreased in an age-dependent manner. We also found PINK1 KO striatal slices had significantly lower basal OCR and decreased ATP levels compared with that of WT controls and this impairment was also age-dependent. Our results suggest that the decrease of DA release may be because of less ATP generation in the PINK1 KO mice. In addition, we also developed a method for direct measurement of mitochondrial respiration in acute striatal slices that could be used in other rodent models.

Unlike the PINK1-deficient *Drosophila* model where there occurs degeneration of DAergic neurons (Clark et al., 2006; Park et al., 2006), all published genetically engineered mice lacking the PINK1 gene have no significant or very mild PD-related phenotype and show normal numbers of DA neurons and no DAergic neurodegeneration (Kitada et al., 2007, 2009). Recently, PINK1 KO rats showed progressive movement deficits and loss of DA neurons when examined at the age of 4 months (Dave et al., 2014). Apart from DAergic neurodegeneration, there has been a controversy in terms of striatal DA levels. Two groups showed age-dependent DA loss in the STR of PINK1 KO mice starting from 9 months or 6 months old (Akundi et al., 2011; Gispert et al., 2009), but Dave et al. showed opposite results in the PINK1 KO rat with increased striatal DA content (Dave et al., 2014). All of these data were based on HPLC method which could not tell whether evoked DA release was impaired or not in vivo. Interestingly, Kitada et al. revealed that 1p-evoked DA overflow was significantly decreased in PINK1 KO mice at the age of 2–3 months using amperometric recording method and suggested that the decrease was because of alteration of DAT function (Kitada et al., 2007). A recent study (Sanchez et al., 2014) reported unaltered striatal DA release in PINK1 KO mice at the same age using FSCV method, which is consistent with our finding. Compared with the amperometric method, which tends to have problems with baseline shifts and calibration, FSCV is a more reliable method to measure and compare DA release from different preparations. Using FSCV, we have found that evoked DA release in dorsal striatum was decreased in an age-dependent manner without alterations of DAT function.

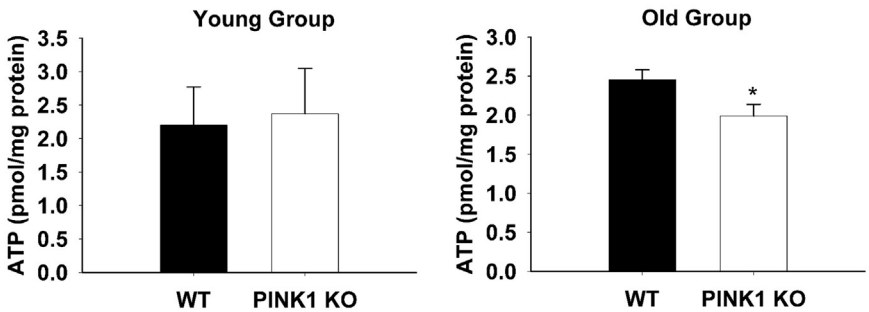

Fig. 5. ATP levels were decreased in PINK1 KO striatal slices from old group. Bar graph showing lower ATP levels in PINK1 KO striatal slices compared with WT in the old age group (N = 7 for each genotype, $^{*}p < 0.05$). ATP levels were not altered in the young age group (N = 4 for each genotype). Abbreviations: PINK1, PTEN-induced kinase 1; KO, knockout; WT, wild-type.

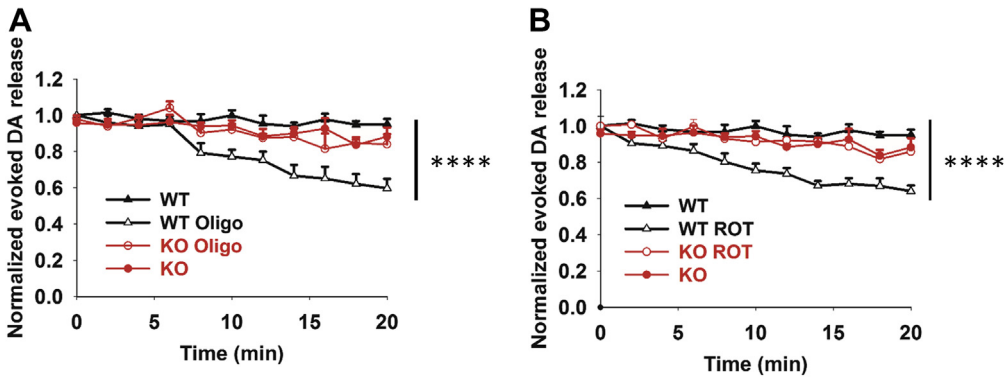

Fig. 6. Inhibition of ATP generation significantly impairs evoked DA release. WT striatal slices were perfused with 10 μM oligomycin (A) or 10 μM rotenone (B) for 20 minutes, and evoked DA release was measured every 2 minutes. Evoked DA release was significantly decreased by the treatment whereas this inhibition was attenuated in the KO slices (N = 3, n = 6. WT vs. WT Oligo, WT vs. WT_ROT, **** $p < 0.0001$, two-way ANOVA). Abbreviations: DA, dopamine; KO, knockout; WT, wild-type.

In our studies, we also measured potassium-evoked DA release to compare the level of total release, which indicates the packing capacity of vesicles and whether there is DA terminal degeneration. We found the total release level was quite similar between genotypes in the young group, while slightly decreased in old PINK1 KO mice but not significant. FCCP-induced DA massive release also showed similar results. These data suggest that aged PINK1 KO mice did not show obvious terminal degeneration and the vesicle packing capacity was normal. This is in consistence with the previous studies (Akundi et al., 2011; Gispert et al., 2009; Kitada et al., 2009; Rappold et al., 2014).

Although dopaminergic neurodegeneration and impairment in DA release were shown to be species specific, the mitochondrial dysfunction was found more generally. The PINK1 KO rats were recently shown to have mitochondrial abnormalities (Villeneuve et al., 2016). These results further demonstrated the causative role of mitochondrial dysfunction in PD. In this study, we found that DA release from aged PINK1 KO striatal slices is more vulnerable to FCCP treatment, suggesting an age-dependent dysfunction of mitochondria. Recently, it has been shown that loss of PINK1 inhibits calcium efflux, leads to mitochondrial calcium overload and mitochondria depolarization (Heeman et al., 2011; Kostic et al., 2015), reduced mitochondrial calcium storage capacity and lower the threshold of opening of the mitochondrial permeability transition pore, which render neurons vulnerable to cell death (Akundi et al., 2011; Gandhi et al., 2009). Our results demonstrated that KO is more vulnerable to FCCP-induced massive DA release. If the mitochondria calcium storage capacity is decreased and MMP is more depolarized in PINK1 KO DA terminals in brain slices, this would lower the threshold for FCCP to deplete the proton gradient of the mitochondrial membrane and the massive DA release. Measure of MMP and mitochondria calcium in DA terminals in striatal slices awaits further exploration in future studies. Abnormal DA homeostasis may contribute to neuronal dysfunction and massive released DA would be accumulatively toxic for DA neurites in the long run.

To investigate the mitochondria function and DA release and their relationship in PINK1 KO mice, we chose Seahorse Extracellular Flux (XF24) analyzer to study the OCR in mouse striatal slices because change in oxygen consumption is an extremely sensitive indicator of mitochondrial function. We found a significant decrease in the basal respiration of aged PINK1 KO mice compared with age matched WT controls. The decreased oxygen consumption could be a result from reduced electron chain complex activity, which in turn could be because of either less mitochondria, less complex content, or impaired complex activity. Previous evidence showed that PINK1 KO mice had normal mitochondrial quantity, average size, and also complex content, but with decreased complex I activity (Gautier et al., 2008; Liu et al., 2011; Morais et al., 2009, 2014). Although in the present study, we did not measure these contents, one of the more probable reasons for the decreased respiration is this complex I dysfunction. We did find that the coupling efficiency was impaired in the KO mice and this impairment started at the young age. In the long run, it may damage mitochondria and cause the reduced respiration rate in the aged group. Our results were consistent with the PINK1 KO rats' data, which showed an elevated proton leak (the opposite way for the coupling efficiency). Unexpectedly, the basal respiration rate, complex I, II, and IV activity were all increased in the isolated mitochondrial analysis from the PINK1 KO rats with the higher proton leak (Villeneuve et al., 2016). This discrepancy could be because of the species difference or because of the isolated mitochondria which are subject to damage and selection during isolation. Our method, using striatal slices, can obtain an undisturbed cellular environment, greater physiological relevance, and little to no artifacts with the rest of the cell preserved. Moreover, mitochondrial coupling efficiency was decreased in the young group, before the DA release decrease, indicating a causative role of the mitochondrial deficit in the DA release.

OCR is an indirect measurement of ATP production, as higher oxygen consumption correlates with increased ATP production. Our respiration results showed significantly reduced basal OCR level and ATP level in the aged KO mice, which is consistent with the data from the patients with PD. We further hypothesize that the age-dependent decrease of DA release may be related to impairment of mitochondrial function, especially the less ATP generation. We inhibited the ATP generation in striatal slices with oligomycin or rotenone and then measured the evoked DA release. As expected, we found both inhibitors could decrease the DA release by around 40% (20 minutes treatment). Longer treatment (i.e., 40 minutes) with oligomycin decreased DA release by around 60%, which confirmed our hypothesis. Gautier et al measured the ATP levels in the STR of both PINK1 KO and WT mice at 3–4 months old and did not find a significant difference (Gautier et al., 2008). Another group found significantly reduced ATP levels under basal conditions in dissociated neurons isolated from PINK1 KO mouse at 6-months old (Gispert et al., 2009). We also measured ATP levels in both young and aged PINK1 KO mice, and observed a significant 25% reduction in ATP levels in aged KO as compared with WT. Consistently, inhibition of DA release by rotenone or oligomycin was blunted in the KO mice. Rotenone has been shown to inhibit DA release via H_2O_2 elevation instead of ATP depletion (Bao et al., 2005; Spanos et al.,

2013). However, we observed a similar suppression of evoked DA release by oligomycin that only inhibits ATP production. Thus, although we could not exclude the possibility that the decreased DA release in KO mice might be because of higher H_2O_2 level, we surmise that the decreased DA release was probably because of less ATP in the old PINK1 KO mice. Interestingly, modification of mitochondrial function could restore pre-existing striatal DA release deficits in PINK1 KO mice (Rappold et al., 2014). DA release is impaired in the MitoPark mouse, in which the mitochondrial transcription factor Tfam is selectively removed in midbrain DA neurons (Good et al., 2011). There are obvious limitations in our study because OCR and ATP were measured from the whole slices and therefore are likely to be activity-independent and coming mostly from inactive MSNs and dopaminergic terminals, as well as astrocytes. Further experimentation will be required to determine whether increasing ATP levels specifically in DA terminals could restore striatal DA release in PINK1 KO mice to normal levels.

Despite these limitations, our work here provides another demonstration linking mitochondrial deficits to decreased DA release in an age-dependent manner in a pre-clinical PD model. The results not only filled the gap in our knowledge between mitochondria and DA neurotransmission but also implied targets for future therapeutic development.

Disclosure

The authors declare no actual or potential conflict interest.

Acknowledgements

We thank Dr. Alpana Singh for critical reading of this manuscript. This work was supported by the National Institute of Neurological Disorders and Stroke (NINDS), United States (NS054773 to C.J. L. and NS098393 to H.Z.) and the Department of Neuroscience at Thomas Jefferson University (Startup Funds to H.Z.).

Appendix A. Supplementary data

Supplementary data to this article can be found online at https://doi.org/10.1016/j.neurobiolaging.2018.10.025.

References

Akundi, R.S., Huang, Z., Eason, J., Pandya, J.D., Zhi, L., Cass, W.A., Sullivan, P.G., Bueler, H., 2011. Increased mitochondrial calcium sensitivity and abnormal expression of innate immunity genes precede dopaminergic defects in Pink1-deficient mice. PLoS One 6, e16038.

Amo, T., Sato, S., Saiki, S., Wolf, A.M., Toyomizu, M., Gautier, C.A., Shen, J., Ohta, S., Hattori, N., 2011. Mitochondrial membrane potential decrease caused by loss of PINK1 is not due to proton leak, but to respiratory chain defects. Neurobiol. Dis. 41, 111–118.

Bao, L., Avshalumov, M.V., Rice, M.E., 2005. Partial mitochondrial inhibition causes striatal dopamine release suppression and medium spiny neuron depolarization via H2O2 elevation, not ATP depletion. J. Neurosci. 25, 10029–10040.

Billups, B., Forsythe, I.D., 2002. Presynaptic mitochondrial calcium sequestration influences transmission at mammalian central synapses. J. Neurosci. 22, 5840–5847.

Brand, M.D., Nicholls, D.G., 2011. Assessing mitochondrial dysfunction in cells. Biochem. J. 435, 297–312.

Clark, I.E., Dodson, M.W., Jiang, C., Cao, J.H., Huh, J.R., Seol, J.H., Yoo, S.J., Hay, B.A., Guo, M., 2006. Drosophila pink1 is required for mitochondrial function and interacts genetically with parkin. Nature 441, 1162–1166.

Cooper, O., Seo, H., Andrabi, S., Guardia-Laguarta, C., Graziotto, J., Sundberg, M., McLean, J.R., Carrillo-Reid, L., Xie, Z., Osborn, T., Hargus, G., Deleidi, M., Lawson, T., Bogetofte, H., Perez-Torres, E., Clark, L., Moskowitz, C., Mazzulli, J., Chen, L., Volpicelli-Daley, L., Romero, N., Jiang, H., Uitti, R.J., Huang, Z., Opala, G., Scarffe, L.A., Dawson, V.L., Klein, C., Feng, J., Ross, O.A., Trojanowski, J.Q., Lee, V.M., Marder, K., Surmeier, D.J., Wszolek, Z.K., Przedborski, S., Krainc, D., Dawson, T.M., Isacson, O., 2012. Pharmacological rescue of mitochondrial deficits in iPSC-derived neural cells from patients with familial Parkinson's disease. Sci. Transl. Med. 4, 141ra190.

Dauer, W., Przedborski, S., 2003. Parkinson's disease: mechanisms and models. Neuron 39, 889–909.

Dave, K.D., De Silva, S., Sheth, N.P., Ramboz, S., Beck, M.J., Quang, C., Switzer 3rd, R.C., Ahmad, S.O., Sunkin, S.M., Walker, D., Cui, X., Fisher, D.A., McCoy, A.M., Gamber, K., Ding, X., Goldberg, M.S., Benkovic, S.A., Haupt, M., Baptista, M.A., Fiske, B.K., Sherer, T.B., Frasier, M.A., 2014. Phenotypic characterization of recessive gene knockout rat models of Parkinson's disease. Neurobiol. Dis. 70, 190–203.

Divito, C.B., Steece-Collier, K., Case, D.T., Williams, S.P., Stancati, J.A., Zhi, L., Rubio, M.E., Sortwell, C.E., Collier, T.J., Sulzer, D., Edwards, R.H., Zhang, H., Seal, R.P., 2015. Loss of VGLut3 produces circadian-dependent hyperdopaminergia and ameliorates motor dysfunction and l-Dopa-mediated dyskinesias in a model of Parkinson's disease. J. Neurosci. 35, 14983–14999.

Fried, N.T., Moffat, C., Seifert, E.L., Oshinsky, M.L., 2014. Functional mitochondrial analysis in acute brain sections from adult rats reveals mitochondrial dysfunction in a rat model of migraine. Am. J. Physiol. Cell Physiol. 307, C1017–C1030.

Gandhi, S., Vaarmann, A., Yao, Z., Duchen, M.R., Wood, N.W., Abramov, A.Y., 2012. Dopamine induced neurodegeneration in a PINK1 model of Parkinson's disease. PLoS One 7, e37564.

Gandhi, S., Wood-Kaczmar, A., Yao, Z., Plun-Favreau, H., Deas, E., Klupsch, K., Downward, J., Latchman, D.S., Tabrizi, S.J., Wood, N.W., Duchen, M.R., Abramov, A.Y., 2009. PINK1-associated Parkinson's disease is caused by neuronal vulnerability to calcium-induced cell death. Mol. Cell 33, 627–638.

Gautier, C.A., Giaime, E., Caballero, E., Nunez, L., Song, Z., Chan, D., Villalobos, C., Shen, J., 2012. Regulation of mitochondrial permeability transition pore by PINK1. Mol. Neurodegener 7, 22.

Gautier, C.A., Kitada, T., Shen, J., 2008. Loss of PINK1 causes mitochondrial functional defects and increased sensitivity to oxidative stress. Proc. Natl. Acad. Sci. U. S. A. 105, 11364–11369.

Gerencser, A.A., Neilson, A., Choi, S.W., Edman, U., Yadava, N., Oh, R.J., Ferrick, D.A., Nicholls, D.G., Brand, M.D., 2009. Quantitative microplate-based respirometry with correction for oxygen diffusion. Anal. Chem. 81, 6868–6878.

Gispert, S., Ricciardi, F., Kurz, A., Azizov, M., Hoepken, H.H., Becker, D., Voos, W., Leuner, K., Muller, W.E., Kudin, A.P., Kunz, W.S., Zimmermann, A., Roeper, J., Wenzel, D., Jendrach, M., Garcia-Arencibia, M., Fernandez-Ruiz, J., Huber, L., Rohrer, H., Barrera, M., Reichert, A.S., Rub, U., Chen, A., Nussbaum, R.L., Auburger, G., 2009. Parkinson phenotype in aged PINK1-deficient mice is accompanied by progressive mitochondrial dysfunction in absence of neurodegeneration. PLoS One 4, e5777.

Good, C.H., Hoffman, A.F., Hoffer, B.J., Chefer, V.I., Shippenberg, T.S., Backman, C.M., Larsson, N.G., Olson, L., Gellhaar, S., Galter, D., Lupica, C.R., 2011. Impaired nigrostriatal function precedes behavioral deficits in a genetic mitochondrial model of Parkinson's disease. FASEB J. 25, 1333–1344.

Hauser, D.N., Hastings, T.G., 2013. Mitochondrial dysfunction and oxidative stress in Parkinson's disease and monogenic parkinsonism. Neurobiol. Dis. 51, 35–42.

Heeman, B., Van den Haute, C., Aelvoet, S.A., Valsecchi, F., Rodenburg, R.J., Reumers, V., Debyser, Z., Callewaert, G., Koopman, W.J., Willems, P.H., Baekelandt, V., 2011. Depletion of PINK1 affects mitochondrial metabolism, calcium homeostasis and energy maintenance. J. Cell Sci. 124 (Pt 7), 1115–1125.

Hewitt, V.L., Whitworth, A.J., 2017. Mechanisms of Parkinson's disease: Lessons from Drosophila. Curr. Top. Dev. Biol. 121, 173–200.

Humpel, C., 2015. Organotypic brain slice cultures: a review. Neuroscience 305, 86–98.

Jiang, C., Agulian, S., Haddad, G.G., 1991. O2 tension in adult and neonatal brain slices under several experimental conditions. Brain Res. 568, 159–164.

Kitada, T., Pisani, A., Porter, D.R., Yamaguchi, H., Tscherter, A., Martella, G., Bonsi, P., Zhang, C., Pothos, E.N., Shen, J., 2007. Impaired dopamine release and synaptic plasticity in the striatum of PINK1-deficient mice. Proc. Natl. Acad. Sci. U. S. A. 104, 11441–11446.

Kitada, T., Tong, Y., Gautier, C.A., Shen, J., 2009. Absence of nigral degeneration in aged parkin/DJ-1/PINK1 triple knockout mice. J. Neurochem. 111, 696–702.

Kostic, M., Ludtmann, M.H., Bading, H., Hershfinkel, M., Steer, E., Chu, C.T., Abramov, A.Y., Sekler, I., 2015. PKA phosphorylation of NCLX reverses mitochondrial calcium overload and depolarization, promoting survival of PINK1-deficient dopaminergic neurons. Cell Rep. 13, 376–386.

Liu, W., Acin-Perez, R., Geghman, K.D., Manfredi, G., Lu, B., Li, C., 2011. Pink1 regulates the oxidative phosphorylation machinery via mitochondrial fission. Proc. Natl. Acad. Sci. U. S. A. 108, 12920–12924.

Moon, H.E., Paek, S.H., 2015. Mitochondrial dysfunction in Parkinson's disease. Exp. Neurobiol. 24, 103–116.

Morais, V.A., Haddad, D., Craessaerts, K., De Bock, P.J., Swerts, J., Vilain, S., Aerts, L., Overbergh, L., Grunewald, A., Seibler, P., Klein, C., Gevaert, K., Verstreken, P., De Strooper, B., 2014. PINK1 loss-of-function mutations affect mitochondrial complex I activity via NdufA10 ubiquinone uncoupling. Science 344, 203–207.

Morais, V.A., Verstreken, P., Roethig, A., Smet, J., Snellinx, A., Vanbrabant, M., Haddad, D., Frezza, C., Mandemakers, W., Vogt-Weisenhorn, D., Van Coster, R., Wurst, W., Scorrano, L., De Strooper, B., 2009. Parkinson's disease mutations in PINK1 result in decreased Complex I activity and deficient synaptic function. EMBO Mol. Med. 1, 99–111.

Narendra, D.P., Youle, R.J., 2011. Targeting mitochondrial dysfunction: role for PINK1 and Parkin in mitochondrial quality control. Antioxid. Redox Signal. 14, 1929–1938.

Park, J., Lee, S.B., Lee, S., Kim, Y., Song, S., Kim, S., Bae, E., Kim, J., Shong, M., Kim, J.M., Chung, J., 2006. Mitochondrial dysfunction in Drosophila PINK1 mutants is complemented by parkin. Nature 441, 1157–1161.

Pathak, D., Shields, L.Y., Mendelsohn, B.A., Haddad, D., Lin, W., Gerencser, A.A., Kim, H., Brand, M.D., Edwards, R.H., Nakamura, K., 2015. The role of mitochondrially derived ATP in synaptic vesicle recycling. J. Biol. Chem. 290, 22325–22336.

Perier, C., Vila, M., 2012. Mitochondrial biology and Parkinson's disease. Cold Spring Harbor Perspect. Med. 2, a009332.

Rappold, P.M., Cui, M., Grima, J.C., Fan, R.Z., de Mesy-Bentley, K.L., Chen, L., Zhuang, X., Bowers, W.J., Tieu, K., 2014. Drp1 inhibition attenuates neurotoxicity and dopamine release deficits in vivo. Nat. Commun. 5, 5244.

Sanchez, G., Varaschin, R.K., Bueler, H., Marcogliese, P.C., Park, D.S., Trudeau, L.E., 2014. Unaltered striatal dopamine release levels in young Parkin knockout, Pink1 knockout, DJ-1 knockout and LRRK2 R1441G transgenic mice. PLoS One 9, e94826.

Schuh, R.A., Clerc, P., Hwang, H., Mehrabian, Z., Bittman, K., Chen, H., Polster, B.M., 2011. Adaptation of microplate-based respirometry for hippocampal slices and analysis of respiratory capacity. J. Neurosci. Res. 89, 1979–1988.

Spanos, M., Gras-Najjar, J., Letchworth, J.M., Sanford, A.L., Toups, J.V., Sombers, L.A., 2013. Quantitation of hydrogen peroxide fluctuations and their modulation of dopamine dynamics in the rat dorsal striatum using fast-scan cyclic voltammetry. ACS Chem. Neurosci. 4, 782–789.

Steer, E.K., Dail, M.K., Chu, C.T., 2015. Beyond mitophagy: cytosolic PINK1 as a messenger of mitochondrial health. Antioxid. Redox Signal. 22, 1047–1059.

Valente, E.M., Abou-Sleiman, P.M., Caputo, V., Muqit, M.M., Harvey, K., Gispert, S., Ali, Z., Del Turco, D., Bentivoglio, A.R., Healy, D.G., Albanese, A., Nussbaum, R., Gonzalez-Maldonado, R., Deller, T., Salvi, S., Cortelli, P., Gilks, W.P., Latchman, D.S., Harvey, R.J., Dallapiccola, B., Auburger, G., Wood, N.W., 2004a. Hereditary early-onset Parkinson's disease caused by mutations in PINK1. Science 304, 1158–1160.

Valente, E.M., Salvi, S., Ialongo, T., Marongiu, R., Elia, A.E., Caputo, V., Romito, L., Albanese, A., Dallapiccola, B., Bentivoglio, A.R., 2004b. PINK1 mutations are associated with sporadic early-onset parkinsonism. Ann. Neurol. 56, 336–341.

van der Merwe, C., van Dyk, H.C., Engelbrecht, L., van der Westhuizen, F.H., Kinnear, C., Loos, B., Bardien, S., 2017. Curcumin rescues a PINK1 knock down SH-SY5Y cellular model of Parkinson's disease from mitochondrial dysfunction and cell death. Mol. Neurobiol. 54, 2752–2762.

Van Laar, V.S., Berman, S.B., 2013. The interplay of neuronal mitochondrial dynamics and bioenergetics: implications for Parkinson's disease. Neurobiol. Dis. 51, 43–55.

Villeneuve, L.M., Purnell, P.R., Boska, M.D., Fox, H.S., 2016. Early expression of Parkinson's disease-related mitochondrial abnormalities in PINK1 knockout rats. Mol. Neurobiol. 53, 171–186.

Wang, H.L., Chou, A.H., Wu, A.S., Chen, S.Y., Weng, Y.H., Kao, Y.C., Yeh, T.H., Chu, P.J., Lu, C.S., 2011. PARK6 PINK1 mutants are defective in maintaining mitochondrial membrane potential and inhibiting ROS formation of substantia nigra dopaminergic neurons. Biochim. Biophys. Acta 1812, 674–684.

Wightman, R.M., Zimmerman, J.B., 1990. Control of dopamine extracellular concentration in rat striatum by impulse flow and uptake. Brain research. Brain Res. Rev. 15, 135–144.

Zhang, H., Sulzer, D., 2003. Glutamate spillover in the striatum depresses dopaminergic transmission by activating group I metabotropic glutamate receptors. J. Neurosci. 23, 10585–10592.